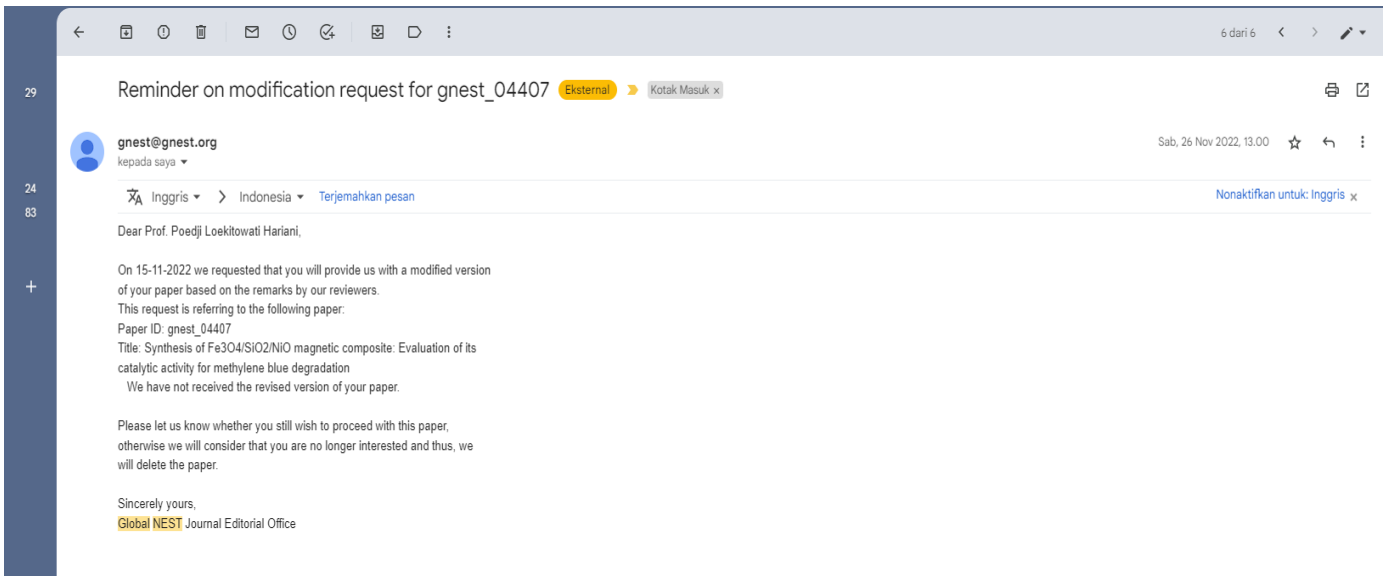Peer rewiew Global Nest Journal, volume 25 issue 2 2023

"Synthesis of $Fe_3O_4/SiO_2/NiO$ magnetic composite: Evaluation of its catalytic activity for methylene blue degradation"

Author: Hariani P.L., Said M., Salni , Rachmat A. , Aprianti N. , and Sthephanie E.A.

Reminder on modification request for gnest_04407 Eksternal Kotak Masuk
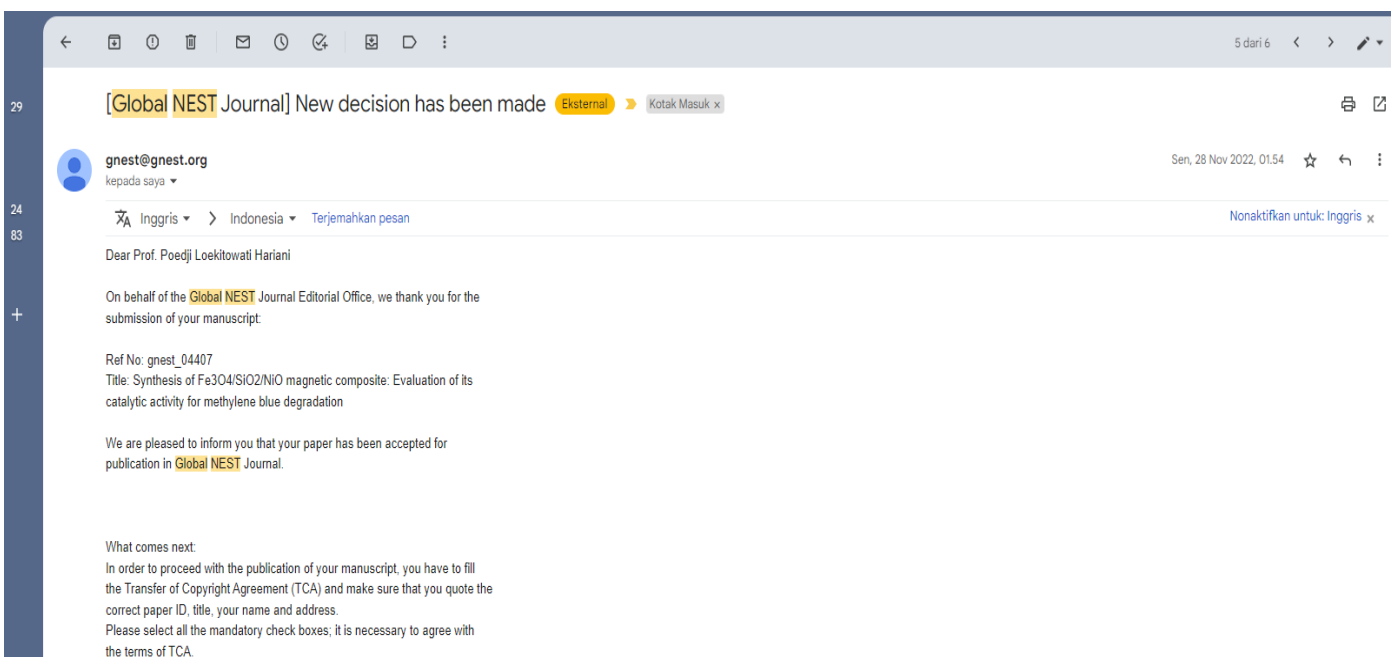
gnest@gnest.org
kepada saya
Sab, 26 Nov 2022, 13.00

Inggris • > Indonesia • Terjemahkan pesan
Nonaktifkan untuk: Inggris

Dear Prof. Poedji Loekitowati Hariani,

On 15-11-2022 we requested that you will provide us with a modified version of your paper based on the remarks by our reviewers.
This request is referring to the following paper:
Paper ID: gnest_04407
Title: Synthesis of Fe3O4/SiO2/NiO magnetic composite: Evaluation of its catalytic activity for methylene blue degradation
  We have not received the revised version of your paper.

Please let us know whether you still wish to proceed with this paper, otherwise we will consider that you are no longer interested and thus, we will delete the paper.

Sincerely yours,
Global NEST Journal Editorial Office

[Global NEST Journal] New decision has been made Eksternal Kotak Masuk

gnest@gnest.org
kepada saya
Sen, 28 Nov 2022, 01.54

Inggris • > Indonesia • Terjemahkan pesan
Nonaktifkan untuk: Inggris

Dear Prof. Poedji Loekitowati Hariani

On behalf of the Global NEST Journal Editorial Office, we thank you for the submission of your manuscript:

Ref No: gnest_04407
Title: Synthesis of Fe3O4/SiO2/NiO magnetic composite: Evaluation of its catalytic activity for methylene blue degradation

We are pleased to inform you that your paper has been accepted for publication in Global NEST Journal.

What comes next:
In order to proceed with the publication of your manuscript, you have to fill the Transfer of Copyright Agreement (TCA) and make sure that you quote the correct paper ID, title, your name and address.
Please select all the mandatory check boxes; it is necessary to agree with the terms of TCA.

After successfully submitting the TCA, you will be allowed to proceed with the payment of the publication fee for Global NEST Journal. The publication fee is 200 euros.

There are two ways you can pay: online and offline.

Online is faster and is performed through a secure network operated by AlphaBank, a Greek bank. We do not keep any records of credit cards or other bank sensitive information on our website and all details kept on our side, are purposed solely for identification and invoicing.

Offline method is performed via Bank transfer. It is slower and you are suggested to follow the instructions on the payment screen.

You can find the TCA form in the link below and you can continue from there.
TCA link: https://journal.gnest.org/node/10412/tca

In case the link above does not function, you can go to "My papers"(https://journal.gnest.org/journal/cmp/author) which is located at the "Author's menu" at the right side of the page.
In the section my papers you can find the link to the Transfer of Copyright Agreement (TCA) for your accepted paper.

If you do not wish to perform the payment yet, you can do at any time by clicking the button "Submit payment" next to the corresponding paper on your "My papers" section once you have agreed with the TCA.
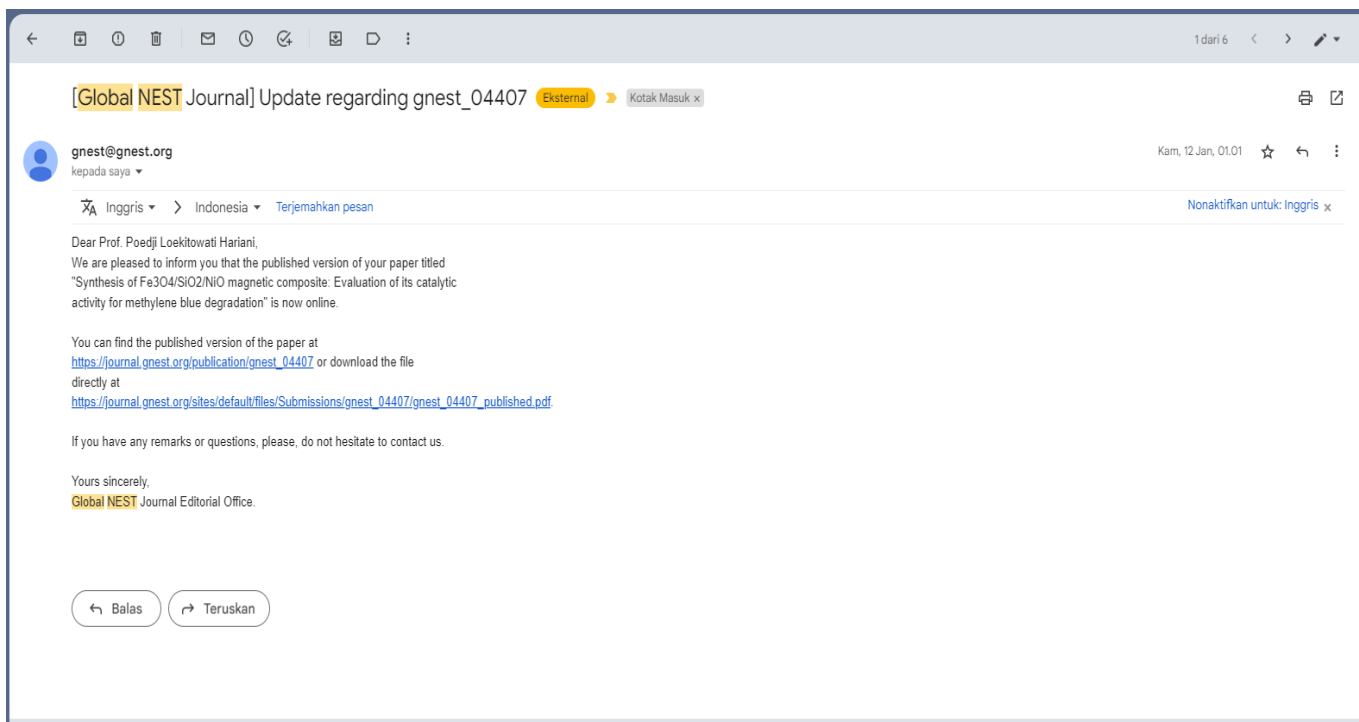
Please, note that both the TCA and the publication fee are required in order to publish your paper.

Yours sincerely,

Global NEST Journal Editorial Office

Global NEST Journal - Invoice and proof of receipt for order 296 Eksternal Kotak Masuk

Global NEST Journal <gnest@gnest.org>
kepada saya
Sen, 28 Nov 2022, 12.35

Inggris > Indonesia Terjemahkan pesan
Nonaktifkan untuk: Inggris

Thank you for selecting Global NEST Journal for your publication.

Please, find attached, the invoice and proof of receipt for the order with id 296.

Kind regards,
Global NEST Secreteriat

2 Lampiran · Dipindai dengan Gmail

PDF invoice_a000000...

PDF proof_a0000001...

Received, thank you.   Well received with thanks.   Thank you I have received it.

gnest@gnest.org
kepada saya ▾

Kam, 12 Jan, 01.01 ☆ ↩ ⋮

文A Inggris ▾ 〉 Indonesia ▾ Terjemahkan pesan
Nonaktifkan untuk: Inggris ✕

Dear Prof. Poedji Loekitowati Hariani,
We are pleased to inform you that the published version of your paper titled
"Synthesis of Fe3O4/SiO2/NiO magnetic composite: Evaluation of its catalytic
activity for methylene blue degradation" is now online.

You can find the published version of the paper at
https://journal.gnest.org/publication/gnest_04407 or download the file
directly at
https://journal.gnest.org/sites/default/files/Submissions/gnest_04407/gnest_04407_published.pdf.

If you have any remarks or questions, please, do not hesitate to contact us.

Yours sincerely,
Global NEST Journal Editorial Office.

↩ Balas   → Teruskan

Dear Author,

The manuscript is on the Synthesis of Fe3O4/SiO2/NiO magnetic composite: Evaluation of its catalytic activity for methylene blue degradation. This research work claims high absorption of the blue dye by the magnetic composite. A few modifications are hereby suggested for improving the manuscript. The authors responded adequately to the comments;

1. English needs to be carefully checked and edited by a native speaker, also pay attention to correct spacing, punctuation, etc, Carefully check that all references are accurate, correctly numbered in thesis format and Check and review the abbreviations.

2. Text, graph and table displays should be uniform (uppercase and lowercase compatibility).

3. In the Introduction, check and mention the allowable limits of all colors of dye in the environment (water bodies, sewerage systems, water reuse, etc.)

4. Authors should address the reasons for using this component based on decolorization.

5. Check and describe the advantages and disadvantages of magnetic metal components.

6. Check the functional groups responsible for adsorption on FT-IR Figure.

7. Check the possibilities of adsorption mechanisms (complexation, pore-filling, precipitation, co-precipitation, etc.) that should be illustrated in a figure.

8. Indicate the mechanism of adsorption by figure with proper description (if available).

9. What changes were observed in the surface morphology and surface area of the material after metal removal?

10. Check and provide some suggestions for future research in this field.

Thank you for reviewing my manuscript with the title "Synthesis of Fe_3O_4/SiO_2/NiO magnetic composite: Evaluation of its catalytic activity for methylene blue degradation". I have fixed it according to the suggestion from the reviewer.

1. English needs to be carefully checked and edited by a native speaker, also pay attention to correct spacing, punctuation, etc, Carefully check that all references are accurate, and correctly numbered in thesis format, and Check and review the abbreviations.

Answer: Thank you for the suggestion. I have checked and edited English and also checked the references

2. Text, graph, and table displays should be uniform (uppercase and lowercase compatibility).

Answer: Thank you. We've changed the text, graph, and tables according to the suggestion (uppercase and lowercase compatibility)

3. In the Introduction, check and mention the allowable limits of all colors of dye in the environment (water bodies, sewerage systems, water reuse, etc.)

Answer: Thank you for the suggestion. The quality standards for wastewater or environment-containing dyes do not exist. In the introduction, the literature shows that a low concentration of dye (< 1 mg/L) can disturb the waters (lines 38).

4. Authors should address the reasons for using this component based on decolorization.

Answer: Thank you. On lines 52-55 it has been explained that the irradiation of the semiconductor by photons on the band gap energy produces positive and negative electrons. The positive hole reacts with a water molecule to produce a hydroxyl radical ($\cdot OH$), while electrons react with O_2 molecules to form superoxide radicals ($\cdot O_2$). The hydroxyl and superoxide radicals degrade dye into smaller non-toxic compounds, CO_2 and H_2O.

5. Check and describe the advantages and disadvantages of magnetic metal components.

Answer: Thank you. We have added the advantage of magnetic metal (Fe_3O_4) as a core in the introduction in lines 71-74, after being used for the photocatalytic degradation process, the composite can easily be separated from the solution using an external magnet, without filtering

6. Check the functional groups responsible for adsorption on FT-IR Figure.

Answer: Thank you for the suggestion. The process that occurs is photocatalytic degradation, not adsorption. There is no change in the FTIR spectra of the composite because the Fe_3O_4/SiO_2/NiO composite as a catalyst

7. Check the possibilities of adsorption mechanisms (complexation, pore-filling, precipitation, co-precipitation, etc.) that should be illustrated in a figure.

Answer: Thank you. We have added the photocatalytic degradation mechanism of methylene blue using composites to the text, lines 251-260

8. Indicate the mechanism of adsorption by the figure with proper description (if available).

Answer: Thank you for the suggestion. We have added the photocatalytic degradation mechanism of methylene blue using Fe_3O_4/SiO_2/NiO composites to the text, lines 251-260, and in the graphical abstract

9. What changes were observed in the surface morphology and surface area of the material after metal removal?
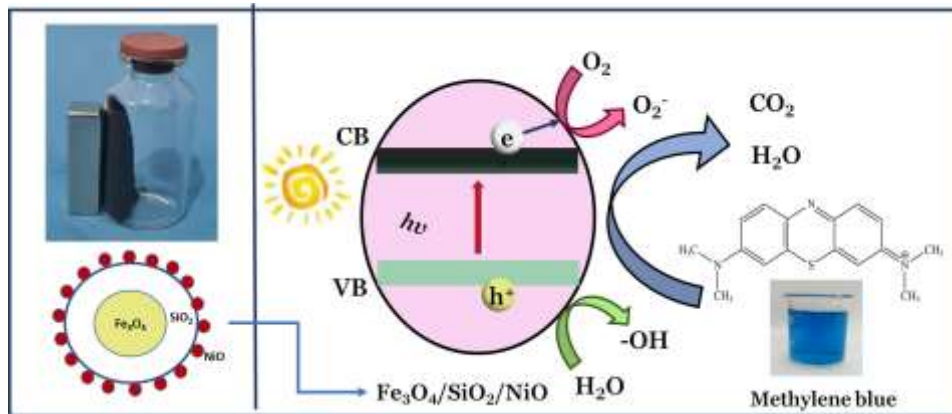
Answer: Thank you. In this study, the mechanism that occurs is the photocatalytic degradation of methylene blue, not metal. The Fe_3O_4/SiO_2/NiO composite functions as a catalyst. The adsorption process only occurs at the beginning before the degradation process.

10. Check and provide some suggestions for future research in this field.

Answer: Thank you. We have added future research in the conclusion (lines 297).

1   **Synthesis of Fe$_3$O$_4$/SiO$_2$/NiO magnetic composite: Evaluation of its catalytic activity for**

2   **methylene blue degradation**

3

4   Poedji Loekitowati Hariani[1*], Muhammad Said[1], Salni[2], Addy Rachmat[1], Nabila Aprianti[3], Erna

5   Amelia Sthephanie[1]

6   [1]Department of Chemistry, Faculty of Mathematics and Natural Sciences, Universitas Sriwijaya,

7   Ogan Ilir, Indonesia

8   [2]Department of Biology, Faculty of Mathematics and Natural Sciences, Universitas Sriwijaya, Ogan

9   Ilir, Indonesia

10   [3]Chemical Engineering Department, Faculty of Engineering, Universitas Sriwijaya, Ogan Ilir,

11   Indonesia

12   [*]Corresponding author:

13   E-mail: *puji_lukitowati@mipa.unsri.ac.id*

14 **Graphical Abstract**

15

16

17

18 **ABSTRACT**

19 Photocatalytic degradation for wastewater treatment is a method that has recently attracted attention.

20 In this research, a synthesized composite of $Fe_3O_4/SiO_2/NiO$ with magnetic properties was used for

21 the photocatalytic degradation of methylene blue dye under UV light. Furthermore, the composites

22 were characterized using XRD, FTIR, BET surface area, SEM-EDS, VSM, and UV-DRS. The results

23 showed that the $Fe_3O_4/SiO_2/NiO$ composite is magnetic with a saturation magnetization of 53.84

24 emu/g. The $Fe_3O_4/SiO_2/NiO$ composite has a surface area of 128.8 m^2/g, large than Fe_3O_4 and

25 Fe_3O/SiO_2. The $Fe_3O_4/SiO_2/NiO$ composite has a band gap of 2.83 eV. The photocatalytic activity of

26 $Fe_3O_4/SiO_2/NiO$ composite against the methylene blue dye exhibited high degradation efficiency

27 reaching 98.51 %. The pseudo-first-order is appropriate to describe the kinetics model of

28 photocatalytic degradation on methylene blue dye . The decrease in the degradation efficiency of the

29 $Fe_3O_4/SiO_2/NiO$ composite after 5 times for the photocatalytic degradation of methylene blue dye

30 from 98.02 % to 94.97 % indicates that the catalyst has high stability. Considering these results, the

31 $Fe_3O_4/SiO_2/NiO$ composites could be used as a potential catalyst in industrial wastewater.

32 **Keywords**: $Fe_3O_4/SiO_2/NiO$, magnetic composite, photocatalytic, degradation, methylene blue dye

1. Introduction

Wastewater discharged from industry often contains pathogenic organisms in organic and inorganic contaminants that harm the environment (Pham *et al.,* 2018). It contains dyes with several characteristics, including a large volume of waste, high chromaticity, high organic matter concentration, poor biodegradability, disturbing aesthetics, and blocking the transmission of sunlight, thereby reducing the photosynthetic activity in the waters. Additionally, a low concentration of dye (< 1 mg/L) can disturb the waters (Vandevivere *et al.,* 1998). Methylene blue ($C_{16}H_{18}ClN_3S$) is a cationic dye widely used in the coloring industry and as a chemical indicator (Khodai *et al.,* 2013; Kuang *et al.,* 2020). It has an aromatic group and a complex structure that is hydrophilic and stable to light, temperature, and chemicals (Hou *et al.,* 2018).

Various technologies, such as biological, physical, and chemical treatment have been used to reduce the concentration of dyes. The methods used to removal dye include adsorption (Ziaadini *et al.,* 2019), precipitation (Ali *et al.,* 2006), coagulation-flocculation (Moghaddam *et al.,* 2010), filtration (David *et al.,* 2020), ozonation (Dias *et al.,* 2019) and others. Adsorption is often applied because it effectively reduces the concentration of dyes but causes secondary pollutants (Fu *et al.,* 2019). Presently, Advanced Oxidation Processes (AOPs) have been an effective method for degrading organic pollutants (Behzadi *et al*., 2020) due to their low cost and high efficiency (Behzadi *et al*., 2020; Jarariya, 2022).

The AOPs method often used is heterogeneous photocatalysis based on semiconductor materials. The irradiation of the semiconductor by photons on the band gap energy produces positive and negative electrons. Furthermore, the positive hole reacts with a water molecule to produce a hydroxyl radical ($\bullet OH$), while electrons react with O_2 molecules to form superoxide radicals ($\bullet O_2$). The hydroxyl and superoxide radicals degrade dye into smaller non-toxic compounds, CO_2 and H_2O (Gao *et al.,* 2013; Salomon *et al.,* 2012). The several semiconductor materials used include TiO_2 (Hou *et al.,* 2018), $NiFe_2O_4$ (Hariani *et al.,* 2021), NiO (Lett *et al.,* 2022), ZnO (Chen *et al.,* 2017), and $CoFe_2O_4$ (Loan *et al.,* 2019).

59   Nickel oxide (NiO) is a p-type transition metal oxide semiconductor with a band gap of about

60   3.5 eV, antiferromagnetic, high conductivity, stable, and catalytic properties (Hosny, 2011; D'Amario

61   *et al.,* 2018; Barakat *et al.,* 2013). It performs effectively in the photodegradation of orange II dye

62   (Khan *et al.,* 2022), methylene blue (Let *et al.,* 2022; Wan *et al.,* 2013), and methyl orange dye

63   (Barzinjy *et al.,* 2020). The combination of magnetic ferrite with NiO is a strategy to increase the

64   efficiency of the catalytic process and the separation of the catalyst from the solution. The magnetic

65   ferrite serves as a core. SiO_2 is a layer to avoid the interaction between NiO and magnetic ferrite. The

66   core-shell-shell structure increases the surface area, reduces the cost of catalyst usage, and increases

67   lifespan (Channei *et al.,* 2014; Girginova *et al.,* 2010). For example, Fe_3O_4 coated with activated

68   carbon and TiO_2 showed better catalytic ability than used with only TiO_2 (Gebrezgiabher *et al.,* 2019).

69   This research synthesized a magnetic composite of $Fe_3O_4/SiO_2/NiO$, with Fe_3O_4 as the core,

70   SiO_2 as the inner shell, and NiO as the outer shell. Fe_3O_4 is the most widely used magnetic iron oxide

71   compared to other ferrite compounds with an inverse spinel structure and superparamagnetic. The

72   advantage of using Fe_3O_4 as a core in composites, after being used for photocatalytic degradation

73   process, the composite can easily be separated from the solution using an external magnet, without

74   filtering. $Fe_3O_4/SiO_2/NiO$ were applied for photocatalytic degradation of methylene blue dye under

75   UV light irradiation. Finally, the kinetic photocatalytic degradation and reusability of these

76   composites were investigated.

77   **2. Materials and methods**

78   *2.1. Materials*

79   The materials used are of analytical grade without purification, including $FeCl_2 \cdot 4H_2O$,

80    $FeCl_3 \cdot 6H_2O$, $FeCl_3 \cdot 6H_2O$, $NiCl_2 \cdot 6H_2O$, NaOH, HCl, C_2H_5OH, NH_4OH, NH_4HCO_3, Tetraethyl

81   orthosilicate (TEOS), Diethylene Glycol (DEG), methylene blue dye purchased from Merck

82   (Germany), distilled water, and N_2 gas.

83

84

85   *2.2. Synthesis of Fe₃O₄*

86   Fe$_3$O$_4$ was synthesized using the coprecipitation method. First, a total of 1.988 g FeCl$_2$·4H$_2$O

87   and 5.406 g FeCl$_3$·6H$_2$O were dissolved in 20 mL of distilled water. Afterward, 1 M NaOH was added

88   to the solution dropwise while slowly stirring with a magnetic stirrer at a speed of 100 rpm, and N$_2$

89   gas was emitted until the pH reached ± 10. The precipitate was separated from the solution using a

90   magnet and washed several times with distilled water and ethanol until the pH was neutral. Finally,

91   it was dried in an oven at 70ºC for 3 hours.

92   *2.3. Synthesis of Fe₃O₄/SiO₂*

93   The Fe$_3$O$_4$/SiO$_2$ was synthesized using the Stober method. First, 0.5 g Fe$_3$O$_4$ was dispersed in

94   20 mL of ethanol using an ultrasonic bath for 30 minutes at room temperature. The obtained product

95   was added 5 mL of ammonia solution (28%), followed by the gradual addition of 2 mL TEOS solution

96   (1 mL TEOS in 20 mL ethanol) using a magnetic stirrer for 3 for 5 hours. The precipitate was washed

97   several times with distilled water and ethanol until the pH was neutral. The Fe$_3$O$_4$/SiO$_2$ were dried in

98   an oven at a temperature of 70ºC for 3 hours.

99   *2.4. Synthesis of Fe₃O₄/SiO₂/NiO*

100   An amount of 0.5 g of NiCl$_2$·6H$_2$O was dispersed in 10 mL of DEG for 30 minutes at room

101   temperature using a water bath sonicator, followed by adding 0.5 g of Fe$_3$O$_4$/SiO$_2$ and 10 mL of

102   0.0025 M NH$_4$HCO$_3$ solution under stirring for 15 minutes. The mixture was transferred to a Teflon

103   autoclave and heated at 120 for 5 hours. The precipitate was washed using distilled water and ethanol.

104   The obtained product was dried in an oven at 70ºC for 3 hours. Finally, it is calcined at a temperature

105   of 300ºC for 2 hours.

106   *2.5. Characterization*

107   The product obtained was identified using an X-ray diffractometer (XRD Panalytical), operated

108   at 40 kV and 30 mA, Cuα (λ = 1.542 Å) as a radiation source, and a range of 2θ at 10-90°. The bond

109   formation was analyzed with Fourier Transform Infra-Red spectroscopy (FTIR, Prestige 21,

110   Shimadzu) at wave numbers of 400-4000 cm^{-1} using the KBr pellet technique. Furthermore, the

specific surface areas were evaluated with N_2 adsorption-desorption using the BET (Quantachrome QuadraWin) method. Scanning electron microscopy with an energy dispersive spectrometer (SEM-EDS JSM 6510) was used to observe surface morphology and elemental composition. Additionally, magnetic properties were evaluated using a Vibrating Sample Magnetometer (VSM Oxford Type 1.2 T). UV-Vis Diffuse Reflectance Spectroscopy (Pharmaspec, UV-1700) was used to determine the band gap at 200-800 nm wavelengths. The concentration of methylene blue dye was determined using a UV-Vis spectrophotometer (Type Orion Aquamate 8000).

2.6. Photocatalytic Activity

Photocatalytic activity of $Fe_3O_4/SiO_2/NiO$ against methylene blue dye under UV light irradiation source (15-W x 3, Philips). In the experiment, 50 mL methylene blue dye at a concentration of 20 mg/L with a 0.5 g/L catalyst dose, the pH of the solution was varied at 5, 6, 7, 8, 9, and 10 using 0.1 M HCl or NaOH. The mixture was stirred in a dark room for 40 minutes to reach equilibrium, followed by a photocatalytic degradation process for 120 minutes (20 minutes intervals). Other variables are catalyst dose (0.25, 0.5, 0.75 and 1.0 g/L) and the dye concentration (10, 20, 30, and 40 mg/L).

The reusability of the catalyst was assessed by magnetically separating it following photocatalytic degradation under optimal conditions. It was then washed using deionized water and dried in an oven for 3 hours at 70°C. Calcination was carried out at 300ºC for ± 2 hours to remove organic substances (Prasad *et al.,* 2022). Finally, the catalyst is reused for photocatalytic degradation and repeated up to 5 times.

3. Results and Discussion

3.1. Catalyst characterization

Fe_3O_4 as the core was synthesized and coated SiO_2 using the coprecipitation and the sol-gel methods, respectively. The $Fe_3O_4/SiO_2/NiO$ was synthesized using the hydrothermal technique. Figure 1 shows that the crystal structure of Fe_3O_4, $Fe_3O_4/SiO_2,$ and $Fe_3O_4/SiO_2/NiO$ were determined using XRD. According to the cubic spinel phase (JCPDS card no. 74-0748), the diffraction

137   characteristics of Fe$_3$O$_4$ were observed at 2θ = 30.39°, 35.69°, 43.35°, 53.87°, 57.65°, and 62.97°.

138   This was appropriate for the planes (220), (311), (400), (422), (511), and (440). After coating with

139   SiO$_2$, a broad peak was observed at 2θ around 23°. This peak is a characteristic of amorphous SiO$_2$

140   (Chen *et al.,* 2014).

141   The new peaks in Fe$_3$O$_4$/SiO$_2$/NiO were observed at 2θ = 76.01° (311) and 80.05° (222).

142   Meanwhile, other peaks overlapped those of Fe$_3$O$_4$, including 37.21° (111), 43.45° (200), and 62.95°

143   (220), according to the structure of JCPDS card no. 78-0423 (NiO). Using the Debye-Scherrer

144   equation, the crystal size of Fe$_3$O$_4$ was calculated to be 7.0 nm, while those of Fe$_3$O$_4$/SiO$_2$ and

145   Fe$_3$O$_4$/SiO$_2$/NiO were 8.2 nm. Another research showed that coating Fe$_3$O$_4$ with SiO$_2$ increased the

146   crystal size from 22.60 to 38.0 nm (Reman *et al.,* 2021).
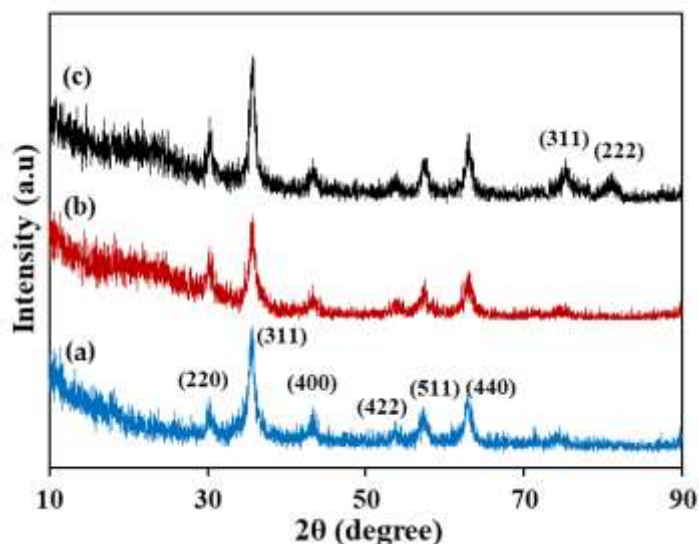
147

148   **Figure 1.** XRD diffraction pattern of (a) Fe$_3$O$_4$, (b) Fe$_3$O$_4$/SiO$_2$, and (c) Fe$_3$O$_4$/SiO$_2$/NiO

149   Figure 2 shows the FTIR spectra of Fe$_3$O$_4$, Fe$_3$O$_4$/SiO$_2$, and Fe$_3$O4/SiO$_2$/NiO. The wave

150   numbers between 3400 cm^{-1} and 1600 cm^{-1} appear in all peaks, indicating the presence of O-H groups

151   from free water, which is absorbed by the catalyst (Hariani *et al.,* 2021; Elzahrani 2017; Ojemaye *et*

152   *al.,* 2017). In Figure 2(a), Fe-O stretching vibration is observed at a wave of 557.43 cm^{-1}. Meanwhile,

153   no other peak was observed apart from water absorption. Figure 2b shows an additional peak at 464.84

154   and 804.31 cm^{-1}, which indicates symmetrical and asymmetrical Si-O terminals (Reman *et al.,* 2021).

155   A strong peak at 1089.78 cm^{-1} is an asymmetric Si-O-Si and Si-O-H vibrational bond observed at a

wave number of 950.60 cm^{-1} (Fu *et al.,* 2019; Han and An, 2021). The wavenumber for metal-oxygen stretching vibration was observed in the 400-700 cm^{-1} range. The absorption band in the 600–700 cm^{-1} indicates absorptions of Ni-O stretching vibration. This study appears at 670.32 cm^{-1}, even though it is not sharp (Qiao *et al.,* 2009).
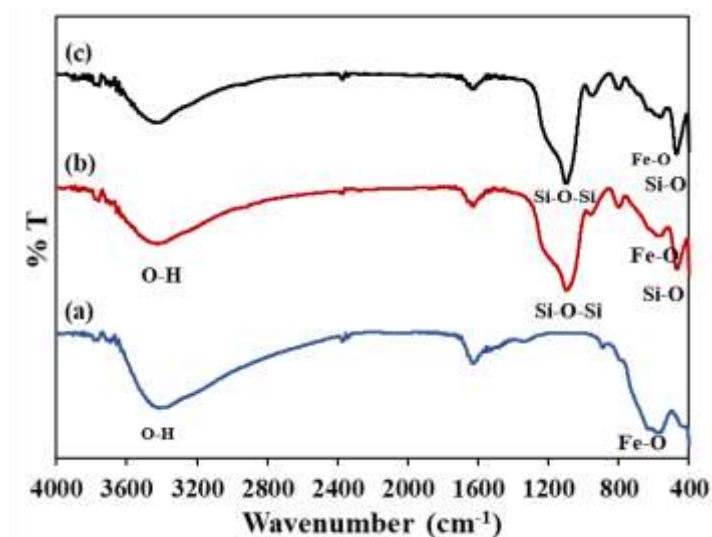
**Figure 2**. FTIR spectra of (a) Fe$_3$O$_4$, (b) Fe$_3$O$_4$/SiO$_2$, and (c) Fe$_3$O$_4$/SiO$_2$/NiO

The surface area affects the catalyst's ability in the degradation process (Kalam *et al.,* 2018). Based on the N$_2$ gas adsorption-desorption curve shown in Figure 3, the specific surface area (S$_{BET}$) of Fe$_3$O$_4$, Fe$_3$O$_4$/SiO$_2$, and Fe$_3$O$_4$/SiO$_2$/NiO were determined using BET analysis. According to the classification IUPAC, all BET curves showed compliance with the Type IV isotherm, namely mesoporous materials. The specific surface area of Fe$_3$O$_4$ (S$_{BET}$) is 88.4 m^2/g, but after coating with SiO$_2$, it becomes 124.2 m^2/g. SiO$_2$ protects it from agglomeration processes, thereby increasing the surface area (Li *et al.,* 2017; Wu *et al.,* 2020). Another research showed that coating Fe$_3$O$_4$ with graphene oxide (GO) produces a larger surface area than Fe$_3$O$_4$ and GO (Thy *et al.,* 2020). In this study, the Fe$_3$O$_4$/SiO$_2$/NiO has a larger surface area than Fe$_3$O$_4$ and Fe$_3$O$_4$/SiO$_2$, which are 128.8 m^2/g. These results are similar to CoFe$_2$O$_4$/SiO$_2$/TiO$_2$, which have a larger surface area than CoFe$_2$O$_4$ and CoFe$_2$O$_4$/SiO$_2$ (Zielińska-Jurek *et al.,* 2017).

174
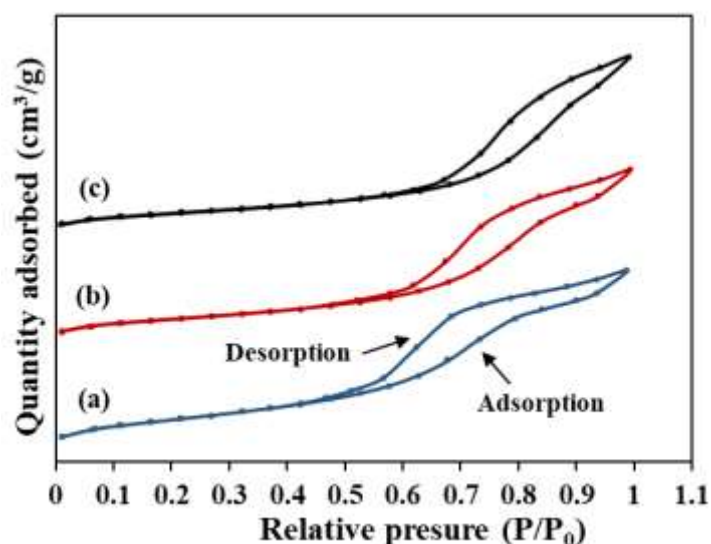
Figure 3. N$_2$ adsorption-desorption isotherm of (a) Fe$_3$O$_4$, (b) Fe$_3$O$_4$/SiO$_2$, and (c) Fe$_3$O$_4$/SiO$_2$/NiO

Figure 4 presents the morphology of Fe$_3$O$_4$, Fe$_3$O$_4$/SiO$_2$, and Fe$_3$O$_4$/SiO$_2$/NiO analyzed using SEM. The Fe$_3$O$_4$ surface appears to be small, dense, and agglomerated, while the Fe$_3$O$_4$/SiO$_2$ and Fe$_3$O$_4$/SiO$_2$/NiO appear to be a granular molecule with reasonably large sizes coating Fe$_3$O$_4$. The SEM mapping of the Fe$_3$O$_4$/SiO$_2$/NiO in Figure 5 shows the distribution of elements on the composite surface. Some parts of the surface indicate the agglomeration of Fe$_3$O$_4$ (red). Meanwhile, Ni (blue) appears to be distributed on the surface of Fe$_3$O$_4$/SiO$_2$ and Fe$_3$O$_4$.
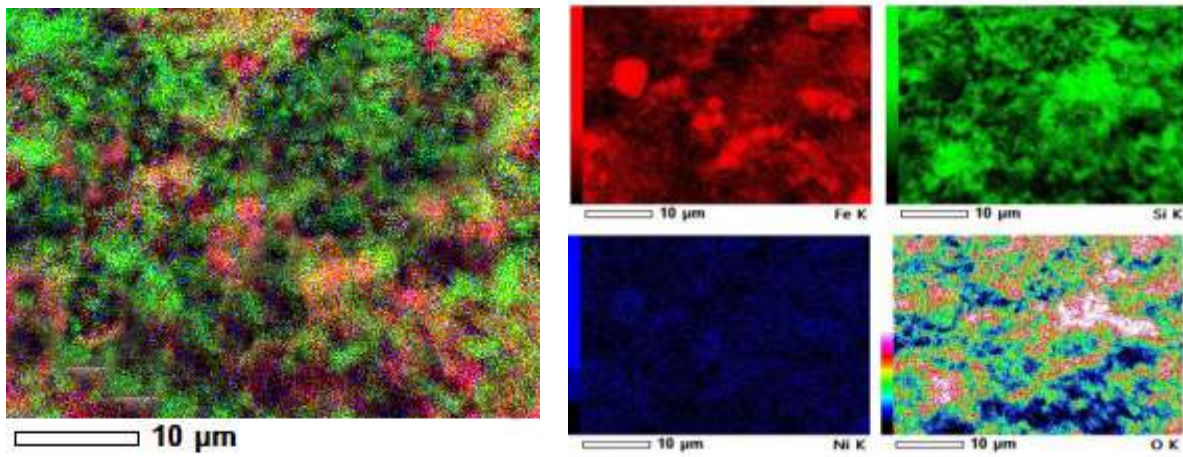

182

183
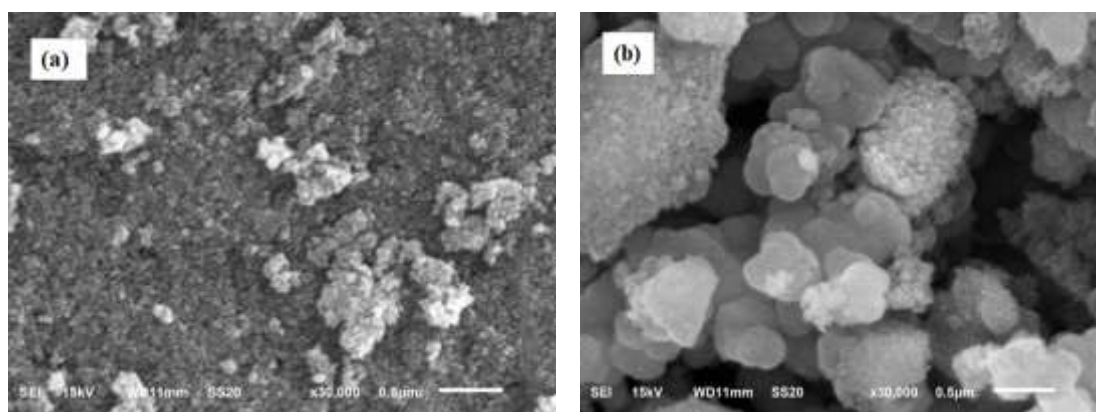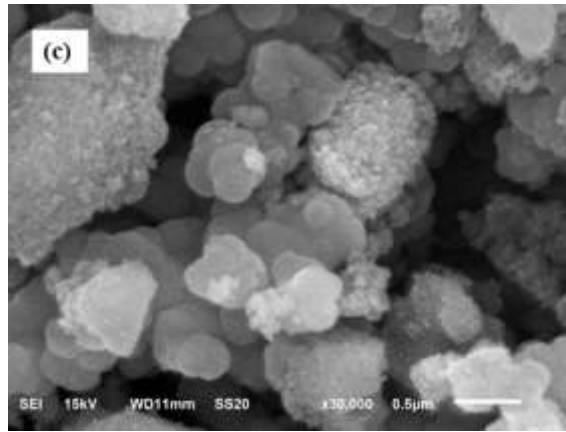
Figure 4. Morphology of (a) Fe_3O_4, (b) Fe_3O_4/SiO_2, and (c) $Fe_3O_4/SiO_2/NiO$

185

Figure 5. SEM Maping of $Fe_3O_4/SiO_2/NiO$

Table 1 shows the composition of Fe_3O_4, Fe_3O_4/SiO_2, and $Fe_3O_4/SiO_2/NiO$ as a result of EDX analysis. The composition of Fe_3O_4 consists of Fe and O, which indicates its purity. The addition of Si to Fe_3O_4/SiO_2 indicates that SiO_2 has successfully to coating Fe_3O_4, while the addition of Ni shows that the element was distributed on the surface of Fe_3O_4/SiO_2.

Table 1. EDX analysis of Fe_3O_4, Fe_3O_4/SiO_2, and $Fe_3O_4/SiO_2/NiO$

Materials	Elements (%)			
	O	Fe	Si	Ni
Fe_3O_4	29.70	70.30	-	-
Fe_3O_4/SiO_2	53.51	18.60	27.89	-
$Fe_3O_4/SiO_2/NiO$	53.28	14.64	23.97	8.11

192

193   Figure 6 shows the magnetic properties of Fe_3O_4, Fe_3O_4/SiO_2, and $Fe_3O_4/SiO_2/NiO$. The Fe_3O_4

194   saturation magnetization of 83.26 emu/g is classified as strong magnetization. Previous research

195   showed that nanomagnetic coating ferrite with non-magnetic materials reduces saturation

196   magnetization. Subsequently, coating Fe_3O_4 with SiO_2 blocks the interaction of the magnetic dipole

197   between adjacent magnetic particles and isolates them from the magnetic field (Kotutha *et al.,* 2019).

198   In general, SiO_2 is non-magnetic, which implies that it is insulating and inert. In this research, the

199   saturation magnetization values of Fe_3O_4/SiO_2 and $Fe_3O_4/SiO_2/NiO$ were 61.96 and 53.84 emu/g,

200   respectively. The presence of NiO reduces the properties of Fe_3O_4/SiO_2. This is related to the surface

201   effect and anisotropy of the particles (Zhao *et al.,* 2015; Sadeghi *et al.,* 2012). The magnetization

202   curve shows a mixture of ferromagnetic and superparamagnetic properties. Therefore, the magnetic

203   properties allow for the easy separation of the composite from the solution after being used for

204   photocatalytic degradation.
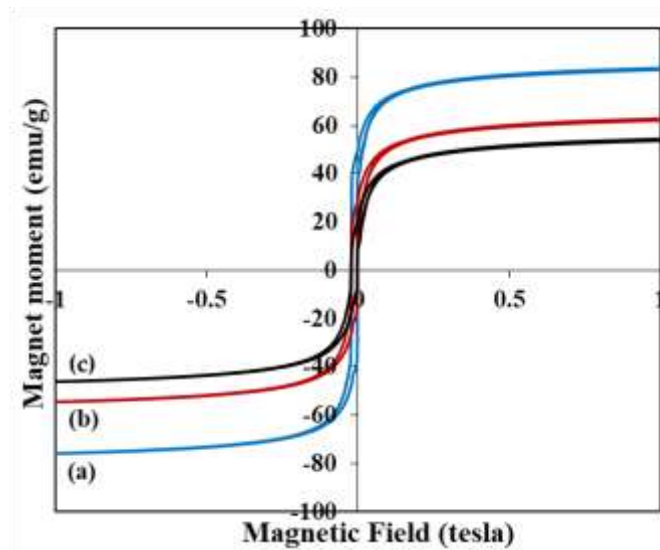
205

206   **Figure 6.** The magnetization of (a) Fe_3O_4, (b) Fe_3O_4/SiO_2 and (c) $Fe_3O_4/SiO_2/NiO$

207   The energy absorbed by the catalyst depends on the optical band gap energy, namely the

208   difference between the valence and conduction bands (Kalam *et al.,* 2018). Figure 7 shows plots

209    $(\alpha h v)^2$ versus Energy (eV) to obtain band gap values of $Fe_3O_4/SiO_2/NiO$. The broad spectrum

210   indicates that Fe_3O_4 dominates the phase in the material. Finally, the band gap value is obtained from

211   Tauc's plot according to the following equation.

$$(\alpha h v)^2 = A(hv - E_g) \tag{1}$$

Where α, A, h, v, and E_g are the absorption coefficient, proportionality constant, Planck's constant, vibrational frequency, and energy band gap. NiO was absorbed in a wavelength of 320 nm. Another research showed that NiO and Fe$_3$O$_4$ were observed at 330 nm and 440 nm, respectively (Barzinjy *et al.,* 2020). In this research, the Fe$_3$O$_4$/SiO$_2$/NiO band gap was 2.83 eV, which is smaller than the band 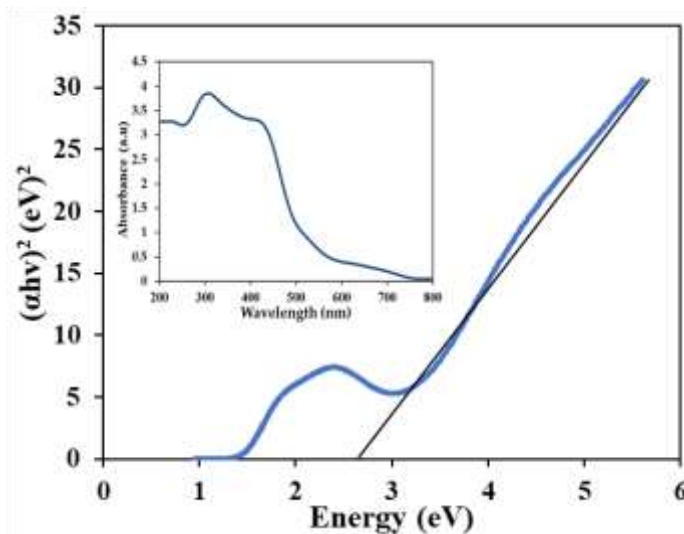gap of NiO ~ 3.5 eV and larger than the band gap of ferrite compounds ~ 2 eV (Hariani *et al.,* 2021). The formation of the core-shell-shell, namely the Fe$_3$O$_4$/SiO$_2$/NiO, successfully reduced the band gap.

Figure 7. Wood-Tauc plot for Fe$_3$O$_4$/SiO$_2$/NiO

3.2. Photocatalytic activity

Figure 8a shows the effect of pH on the efficiency of photocatalytic degradation. The dye concentration was 20 mg/L, and the catalyst dose was 0.5 g/L with a pH varying from 5 to 10. The pH solution contributes to the degradation of dyestuffs and gives a charge to the catalyst's surface. Photocatalytic degradation of methylene blue dye using several catalysts, namely TiO$_2$, ZnO, Co$_3$O$_4$, CdS, and MnTiO$_3$, was optimum at a pH range of 9 to 11 (Alkaykh *et al.,* 2020; Alkaim *et al.,* 2014). Methylene blue dye is a cationic dye at alkaline pH, the dye has a positive charge, and the interaction is more effective with a negatively charged catalyst. Furthermore, there are many OH⁻ ions at the pH of alkaline solutions. The catalyst absorbs irradiation to produce holes (h_{VB}^+) which then react with

231   OH⁻ to form hydroxyl radicals (•OH). At high pH, hydroxyl radicals are quickly scavenged, giving

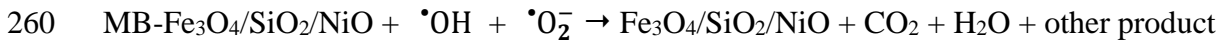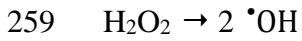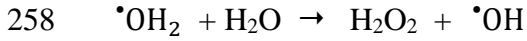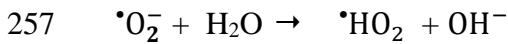232   them no opportunity to react with dyes (Alkaim *et al.,* 2014).
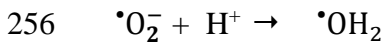

233

234
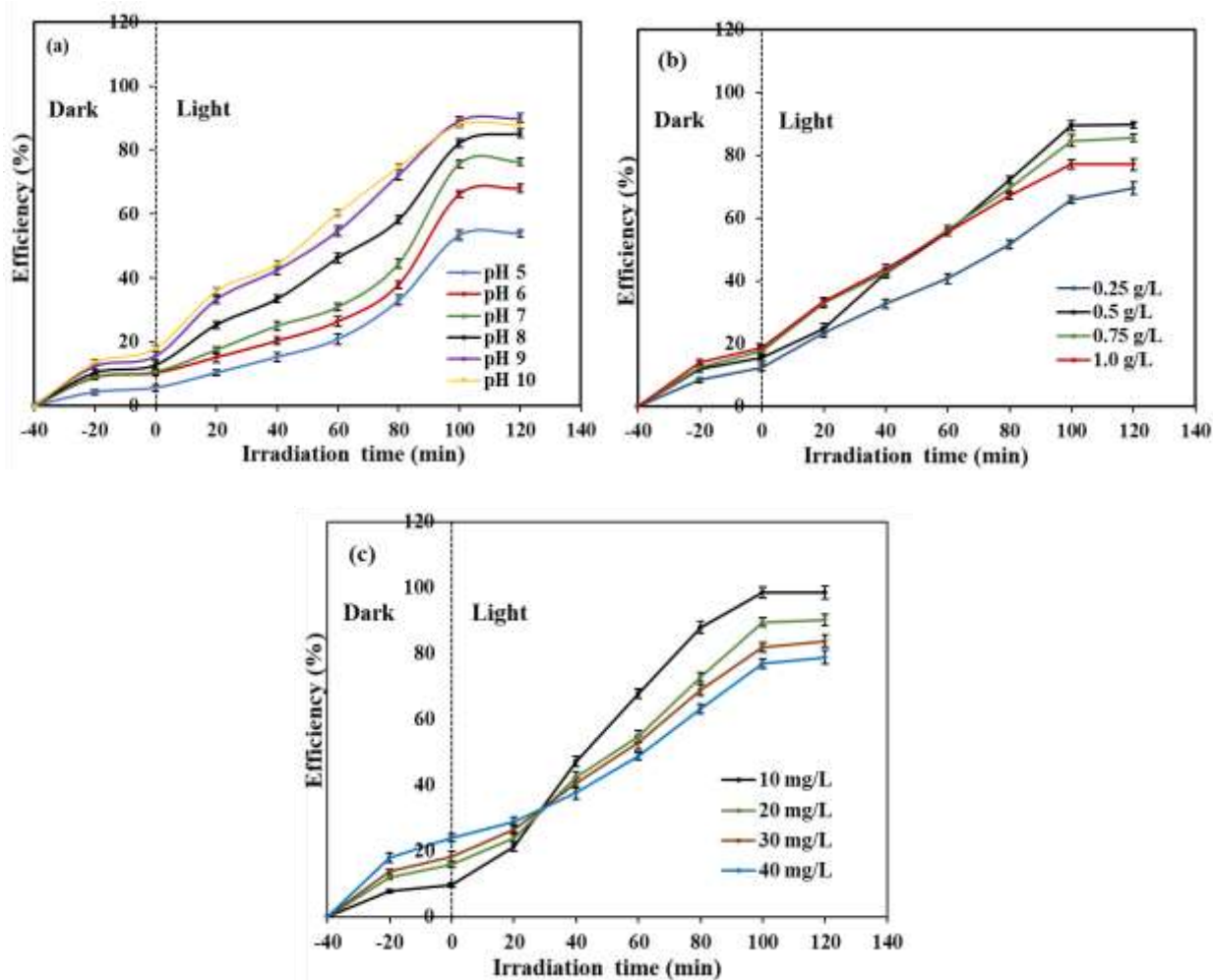
235   **Figure 8**. Effect of (a) pH solution, (b) catalyst dose, and (c) initial concentration of dye on the

236   photocatalytic degradation of the $Fe_3O_4/SiO_2/NiO$

237   The effect of catalyst doses was conducted with variations of 0.25, 0.5, 0.75, and 1.0 g/L, while

238   the concentration was 20 mg/L at a pH of 9. Figure 8b shows that the higher the amount of catalyst,

239   the more the dye degraded. In addition to being observed at 100 minutes, doses of 0.5 and 0.75 g/L

240   had nearly the same degradation rate. However, there was a decrease at 1.0 g/L. At higher doses, there

241   is a reduction in the reaction rate due to catalyst loading, which causes the deactivation of activated

242   molecules by collision with ground state catalysts (Herman, 1995). Furthermore, the optimum dose

243   was at 0.5 g/L with a dye reduction efficiency of 89.77% in 100 minutes.

244   The effect of the initial dye concentration was analyzed using 10 to 50 mg/L. Figure 8c shows

245   that the dye reduction efficiency increased directly with the initial dye concentration after 100 min.

246   It also increases with the number of dye molecules adsorbed on the catalyst surface. This prevents

247   photons from reaching the catalyst surface as they are blocked by the dye (Hariani *et al.,* 2022;

248   Makeswari and Saraswathi, 2020). Therefore, the photocatalytic degradation of methylene blue dye

249   was better at a low concentration of 10 mg/L with an efficiency of 98.51%. This indicates that the

250   catalyst plays a significant role in dye degradation.

251   The mechanism of photocatalytic degradation of methylene blue (MB) dye using $Fe_3O_4/SiO_2/NiO$

252   according to the reaction: (Ammar *et al*., 2020).

253    $Fe_3O_4/SiO_2/NiO + hv \rightarrow Fe_3O_4/SiO_2/NiO\ (e_{CB}{}^- + h_{VB}{}^+)$

254    $e_{CB}{}^- + O_2 \rightarrow {}^\bullet O_2^-$

255    $h_{VB}{}^+ + H_2O \rightarrow {}^\bullet OH + H^+$

256    ${}^\bullet O_2^- + H^+ \rightarrow {}^\bullet OH_2$

257    ${}^\bullet O_2^- + H_2O \rightarrow {}^\bullet HO_2 + OH^-$

258    ${}^\bullet OH_2 + H_2O \rightarrow H_2O_2 + {}^\bullet OH$

259    $H_2O_2 \rightarrow 2\ {}^\bullet OH$

260    $MB\text{-}Fe_3O_4/SiO_2/NiO + {}^\bullet OH + {}^\bullet O_2^- \rightarrow Fe_3O_4/SiO_2/NiO + CO_2 + H_2O + other\ product$
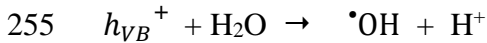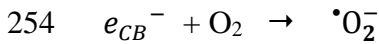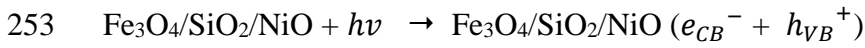
261   *3.3. Kinetic for photodegradation*

262   The following formula expresses the kinetic model of photocatalytic degradation on methylene

263   blue dye using pseudo-first-order:

$$\ln C_0/C_t = kt \tag{2}$$

265   Where C_0 and C_t are the initial concentration at each time (a certain time) (mg/L), t is the irradiation

266   time (min), and k is the rate constant (min^{-1}). The k value is obtained from the slope of the linear

267   fitting graph $\ln C_0/C_t$ Versus t. This research determined the kinetics of photocatalytic degradation

268   using a methylene blue dye concentration of 10 mg/L, a catalyst dose of 0.5 g/L, and a solution pH

269   of 9 (Figure 9). The coefficient of determination value ($R^2 = 0.990 > 0.9$) indicates that the kinetic

270   model is compatible (Van *et al*., 2019). Therefore, the k value obtained is $1.1.10^{-4}$ min^{-1}.

271
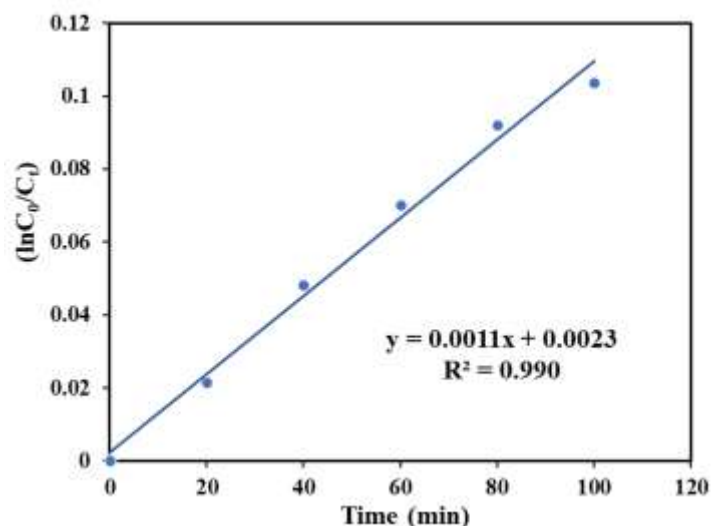
Figure 9. The plot of the pseudo-first-order for photocatalytic degradation on methylene blue dye

3.4. Reusability of Fe₃O₄/SiO₂/NiO

Reusability is essential for the remediation process as it aims to see the cost-effectiveness and feasibility of catalysts (Gebrezgiabher *et al.,* 2019; Moosavi *et al.,* 2020). Its performance uses methylene blue dye concentration of 10 mg/L, a dose of 0.5 g/L, and a solution of pH 9. Figure 10 shows the efficiency of photocatalytic degradation after 5 cycles. Subsequently, the efficiency of photocatalytic degradation decreased from 98.02 to 94.97% ($< 5\%$). The photocatalyst properties, such as surface area, number of active sites, and the presence of impurities, could change during reuse, but those with approximately 5 cycles continue to show good performance. It can be believed that the Fe₃O₄/SiO₂/NiO exhibits excellent photocatalyst stability.
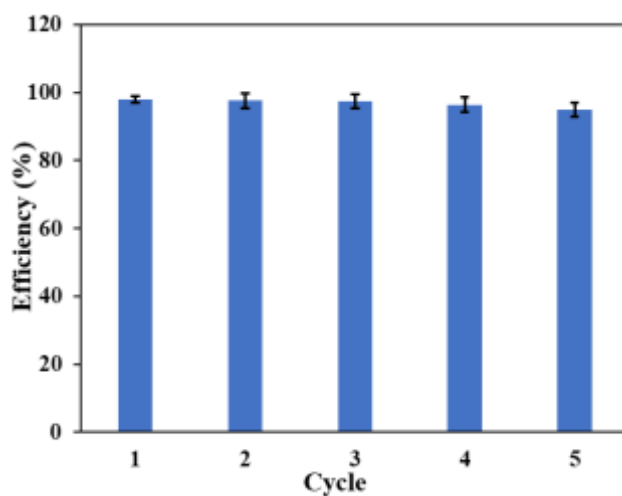
Figure 10. Reusability of Fe₃O₄/SiO₂/NiO

284   Table 2 shows a degradation efficiency comparison of methylene blue dye using several catalysts.

285   The results of this research have high degradation efficiency with the same initial concentration and

286   relatively fast time.

287   **Table 2.** Photocatalytic degradation efficiency of some catalysts againts methylene blue dye

Catalyst	Initial concentration (mg/L)	Irradiation time (min)	Efficiency (%)	References
$Cu-TiO_2/ZnO$	35	120	64.72	Khaki *et al.*, (2017)
$SnS_2-SiO_2@\alpha-Fe_2O_3$	5	100	96.0	Balu et al., (2018)
$ZnO-SnO_2$	10	60	96.53	Lin et al., (2018)
$TiO_2/Alg/FeNPs$	5	120	97.6	Kanakaraju *et al.,* (2018)
$CoFe_2O_4/H_2O_2$	10	140	82.0	Kalam *et al.*, (2018)
$Fe_3O_4@SiO_2@CeO_2$	10	50	98.0	Ziaadini *et al.*, (2019)
$CoFe_2O_4@SiO_2@DyCe_2O_7$	20	30	94.5	Zinatloo-Ajabshir and Salavati-Niasari (2019)
Fe_2TiO_5	10	250	97.0	Vasiljevic *et al.*, (2020)
$Fe_3O_4/SiO_2/NiO$	10	100	98.51	Present study

288

289   **4. Conclusion**

290   The core-shell-shell composite $Fe_3O_4/SiO_2/NiO$ has been successfully synthesized, with Fe_3O_4

291   as the core, SiO_2 as the interlayer, and NiO spread on the composite surface. The composite has

292   magnetic properties with a saturation magnetization value of 53.84 emu/g. Furthermore, the optimum

293   conditions for photocatalytic degradation of $Fe_3O_4/SiO_2/NiO$ against methylene blue dye were pH 9,

294   catalyst dose of 0.5 g/L, 10 mg/L dye concentration, and irradiation time of 100 minutes, the

295 degradation efficiency of 98.51%. This composite has high stability, and reusability of approximately

296 5 cycles decreases the removal efficiency by < 5%. Therefore, the $Fe_3O_4/SiO_2/NiO$ composite has the

297 potential to reduce water pollution. ==Further research needs to be developed for the photocatalytic==

298 ==degradation of wastewater containing other pollutants.==

303 **References**

304 Ali M., Sarkar A., Pandey M.D. and Pandey S. (2006), Efficient precipitation of dyes from dilute

305   aqueous solutions of ionic liquids, *Analytical sciences*, **22**, 1051–1053.

306 Alkaim A.F., Aljeboree A.M., Alrazaq N.A., Baqir S.J., Hussein F.H. and Lili A.J. (2014), Effect of

307   pH on adsorption and photocatalytic degradation efficiency of different catalyst on removal of

308   Methylene blue, *Asian Journal of Chemistry*, **26**, 8445–8448.

309 Alkaykh S., Mbarek A. and Ali-Shattle E.E. (2020), Photocatalytic degradation of methylene blue

310   dye in aqueous solution by $MnTiO_3$ nanoparticles under sunlight irradiation, *Heliyon*, **6**, 1–6.

311 Ammar S.H., Elaibi A.I., and Mohamme I.S. (2020), Core/shell $Fe_3O_4@Al_2O_3$-PMo magnetic

312   nanocatalyst for photocatalytic degradation of organic pollutants in an internal loop airlift reactor,

313   *Journal of Water Process Engineering*, **37**, 1–11

314 Balu S, Uma K., Pan G.T., Yang T.C. and Ramaraj S.K. (2018), Degradation of methylene blue dye

315   in the presence of visible light using $SiO_2@\alpha\text{-}Fe_2O_3$ nanocomposites deposited on SnS_2 flowers,

316   *Materials*, **6**, 1030.

317 Barakat A., Al-Noaimi M., Suleiman M., Aldwayyan A.S., Hammouti B., Hadda T.B., Haddad S.F.,

318   Boshaala A. and Warad I. (2013), One Step Synthesis of NiO Nanoparticles via Solid-State

319   Thermal Decomposition at Low-Temperature of Novel Aqua (2,9-dimethyl-1,10-
320   phenanthroline) $NiCl_2$ Complex, *International Journal of Molecular Sciences*, **14**, 23941–23954.

321   Barzinjy A.A., Hamad S.M., Aydin S., Ahmed M.H. and Hussain F.H.S. (2020), Green and eco-
322   friendly synthesis of Nickel oxide nanoparticles and its photocatalytic activity for Methyl orange
323   degradation, *Journal of Materials Science: Materials in Electronics*, **31**, 11303–11316.

324   Behzadi S., Nonahal B., Royaee S.J. and Asadi A.A. (2020), $TiO_2/SiO_2/Fe_3O_4$ magnetic nanoparticles
325   synthesis and application in Methyl orange UV photocatalytic removal, *Water Science and*
326   *Technology*, **11**, 2432–2445.

327   Channei D., Inceesungvorn B., Wetchakun N. and Phanichphant S. (2014), Synthesis of
328    $Fe_3O_4/SiO_2/CeO_2$ core–shell magnetic and their application as photocatalyst, *Journal of*
329   *Nanoscience and Nanotechnology*, **14**, 7756–7762.

330   Chen F., Yan F., Chen Q., Wang Y., Han L., Chen Z. and Fang S. (2014), Fabrication of
331    $Fe_3O_4@SiO_2@TiO_2$ nanoparticles supported by graphene oxide sheets for the repeated
332   adsorption and photocatalytic degradation of rhodamine B under UV irradiation, *Dalton*
333   *Transactions*, **43**, 13537–13544.

334   Chen X., Wu Z., Liu D. and Gao. (2017), Preparation ZnO photocatalyst for the efficient and rapid
335   photocatalytic degradations of azo dyes, *Nanoscale Research Letters*, **12**, 143.

336   David P.S., Karananithi A. and Fathima N.N. (2020), Improved filtration for dye removal using
337   keratin-polymide blend nanofibrous membranes*, Environmental Science and Pollution*
338   *Research*, **27**, 45629–45638.

339   Dias N.C., Bassin J.P. and Sant'Anna G.L. (2019), Ozonation of the dye reactive red 239 and
340   biodegradation of ozonation products in a moving-bed biofilm reactor: revealing reaction
341   products and degradations pathways, *International Biodeterioration & Biodegradation*, **144**, 1–
342   9.

343 D'Amario L., Fohlinger J., Boschloo G. and Hammarstrom L. (2018), Unveiling hole trapping and
344   surface dynamics of NiO nanoparticles, *Chemical Science*, **9**, 223–230.

345 Elzahrani E. (2017), Photodegradation of binary azo dyes using core-shell $Fe_3O_4/SiO_2/TiO_2$
346   nanospheres, *American Journal of Analytical Chemistry*, **8**, 95–115.

347 Fu C., Liu X., Wang Y., Li L. and Zhang Z. (2019), Preparation and characterization of
348     $Fe_3O_4@SiO_2@TiO_2$-Co/rGO magnetic visible light photocatalyst for water treatment, *RSC*
349   *Advances*, **9**, 20256–20265.

350 Gao P., Liu J., Sun D.D. and Ng W. (2013), Graphene oxide-CdS composite with high photocatalytic
351   degradation and disinfection activities under visible light irradiation, *Journal of Hazardous*
352   *Materials*, **250**, 412–2420.

353 Gebrezgiabher M., Gebreslassie G., Gebretsadik T., Yeabyo G., Elemo F., Bayeh Y., Thomas M. and
354   Linert W. (2019), AC-Doped TiO_2/Fe_3O_4 nanocomposite for photocatalytic dye degradation
355   under natural sunlight irradiation, *Journal of Composites Science*, **3**, 75.

356 Girginova P.I., Daniel-da-Silva A.L., Lopes C.B., Figueira P., Otero M., Amaral V.S., Pereira E. and
357   Trindade T. (2010), Silica coated magnetite particles for magnetic removal of Hg^{2+} from water,
358   *Journal of Colloid and Interface Science*, **345**, 234–240.

359 Han J.S. and An G.S. (2021), Preparation of Dual-Layered Core–Shell $Fe_3O_4@SiO_2$ nanoparticles
360   and their properties of plasmid DNA purification, *Nanomaterials*, **11**, 3422.

361 Hariani P.L., Said M., Rachmat A., Riyanti F., Pratiwi H.C. and Rizki W.T. (2021), Preparation of
362     $NiFe_2O_4$ nanoparticles by solution combustion method as photocatalyst of congo red, *Bulletin of*
363   *Chemical Reaction Engineering & Catalysis*, **16**, 481–490.

364 Hariani P.L., Said M., Salni, Aprianti N. and Naibaho Y.A.L.R. (2022), High efficient photocatalytic
365   degradation of methyl orange dye in an aqueous solution by $CoFe_2O_4$-SiO_2-TiO_2 magnetic
366   catalyst, *Journal of Ecological Engineering*, **23**, 118–128.

367   Herman, J.M. (1995), Heterogeneous photocatalysis; an emerging discipline involving multiphase
368   system, *Catalyst Today*, **24**, 157–164.

369   Hosny N.M. (2011), Synthesis, characterization and optical band gap of NiO nanoparticles derived
370   from anthranilic acid and precursors via a thermal decomposition route, *Polyhedron*, **30**, 470–
371   476.

372   Hou C., Hu B. and Zhu J. (2018), Photocatalytic degradation of methylene blue over TiO_2 Pretreated
373   with varying concentrations of NaOH, *Catalysts*, **8**, 575.

374   Jarariya R. (2022), A review based on spinel ferrite nanomaterials $MgFe_2O_4$ - synthesis of
375   photocatalytic dye degradation in visible light response, *Journal of Environmental Treatment*
376   *Techniques*, **10**, 149–2156.

377   Kanakaraju D., Shahdad N.R.M., Lim Y. and Pace. A. (2018), Magnetic hybrid TiO_2/Alg/FeNPS
378   triads for the efficient removal of Methylene blue from water, *Sustainable Chemistry and*
379   *Pharmacy*, **8**, 50–62.

380   Kalam A., Al-Sehemi A.G., Assiri M., Du G., Ahmad T., Ahmad I. and Pannipara M. (2018),
381   Modified solvothermal synthesis of cobalt ferrite ($CoFe_2O_4$) magnetic nanoparticles
382   photocatalysts for degradation of Methylene blue with H_2O_2/visible light, *Results in Physics*, **8**,
383   1046–1053.

384   Khaki M.R.D., Shafeeyan M.S., Raman A.A.A. and Daud W.M.A.W. (2017), Evaluating the
385   efficiency of nano-sized Cu doped TiO_2/ZnO photocatalyst under visible light irradiation,
386   *Journal of Molecular Liquids*, **258**, 354–365.

387   Khan N.A., Saeed K., Khan I., Gul T., Sadiq M., Uddin A. and Zekker I. (2022), Efficient
388   photodegradation of orange II dye by nickel oxide nanoparticles and nanoclay supported nickel
389   oxide nanocomposite, *Applied Water Science*, **12**, 1–10.

390   Khodai M., Ghasemi N., Moradi B. and Rahimi M. (2013), Removal of methylene blue from

391   wastewater by adsorption onto $ZnCl_2$ activated corn husk carbon equilibrium studies, *Journal of*

392   *Chemistry*, **3**, 1–7.

393   Kotutha I., Duangchuen T., Swatsitang K., Meewasana W., Khajonrit J. and Maensiri S. (2019),

394   Electrochemical properties of $rGO/CoFe_2O_4$ nanocomposites for energy storage application,

395   *Ionics*, **25**, 5401–5409.

396   Kuang Y., Zhang X. and Zhou S. (2020), Adsorption of methylene blue in water onto activated carbon

397   by surfactant modification, *Water*, **12**, 587.

398   Lett J.A., Sagadevan S., Weldegebrieal G.K. and Fatimah I. (2022), Hydrothermal synthesis and

399   photocatalytic activity of NiO nanoparticles under visible light illumination, *Bulletin of Chemical*

400   *Reaction Engineering & Catalysis*, **17**, 2, 340–349.

401   Lin J., Luo Z., Liu J. and Li, P. (2018), Photocatalitic degradation of methylene blue in aqueous

402   solution by using $ZnO\text{-}SnO_2$ nanocomposites, *Materials Science in Semiconductor Processing*,

403   **87**, 24–31.

404   Li Q., Lu C., Chen C., Xie L., Liu Y., Li Y., Kong Q. and Wang H. (2017), Layered $NiCo_2O_4/$ reduced

405   graphene oxide composite as an advanced electrode for supercapacitor, *Energy Storage*

406   *Materials*, **8**, 59–67.

407   Loan N.T.T, Hien Lan N.T.H, Hang N.T.T, Hai N.Q, Anh D.T.T, Hau V. T, Tan, L.V. and Tran T.V.

408   (2019), $CoFe_2O_4$ nanomaterials: effect of annealing temperature on characterization, magnetic,

409   photocatalytic, and photo-Fenton properties, *Processes*, **7**, 885.

410   Makeswari M. and Saraswathi, P. (2020), Photocatalytic degradation of methylene blue and methyl

411   orange from aqueous solution using solar light onto chitosan bi-metal oxide composite, *SN*

412   *Applied Sciences*, **2**, 336.

413   Moghaddam S.S., Moghaddam M.R.A. and Arami M. (2010), Coagulation/flocculation process for

414   dye removal using sludge from water treatment plant: optimization through response surface

415   methodology, *Journal of Hazardous Materials*, **175**, 651–657.

416   Moosavi S., Li R.Y.M., Lai C.W., Yusof Y., Gan S., Akbarzadeh O., Chowhury Z.Z., Yue X.G. and

417   Johan M.R. (2020), Methylene blue dye photocatalytic degradation over synthesized

418        $Fe_3O_4/AC/TiO_2$ nano-catalyst: degradation and reusability studies, *Nanomaterials*, **10**, 2360.

419   Ojemaye M.O., Okoh O.O. and Okoh A.I. (2017), Performance of $NiFe_2O_4$-SiO_2-TiO_2 photocatalyst

420   for the effective photocatalytic re-duction of Cr(VI) from aqueous solutions, *Journal of*

421   *Nanomaterials*, **2017**, 1–18.

422   Pham T.D., Bui T.T., Nguyen V.T., Bui T.K.V., Tran T.T., Phan Q.C., Pham T.D. and Hoang T.H.

423   (2018), Adsorption of polyelectrolyte onto nanosilica synthesized from rice husk: characteristics,

424   mechanisms, and application for antibiotic removal, *Polymers*, **10**, 220.

425   Prasad K.S. and Shamshuddin S.Z.M. (2022), Highly efficient conversion of glycerol and t-butanol

426   to biofuel additives over AlPO solid acid catalyst under microwave irradiation technique: kinetic

427   study, *Comptes Rendus Chimie*, **25**, 149–170.

428   Qiao H., Wei Z., Yang H., Zhu L. and Yan X. (2009), Preparation and characterization of NiO

429   nanoparticles by anodic arc plasma method, *Journal of Nanomaterials*, **2009**, 1–5.

430   Reman G,U., Tahir M., Goh P.S., Ismail A.F., Hafeez A. and Khan I.U. (2021), Enhancing the

431   photodegradation of phenol using Fe_3O_4/SiO_2 binary nanocomposite mediated by silane agent,

432   *Journal of Physics and Chemistry of Solids*, **153**, 110022.

433   Sadeghi S., Azhdari H., Arabi H. and Moghaddam A.Z. (2012), Surface modified magnetic Fe_3O_4

434   nanoparticles as a selective sorbent for solid phase extraction of uranyl ions from water sampels,

435   *Journal of Hazardous Materials*, **215**, 208–216.

436 Salomon R.V., Lydia I.S., Merlin J.P. and Venuvalingam P. (2012), Enhanced photocatalytic

437   degradation of azo dye using nano Fe$_3$O$_4$, *Journal of the Iranian Chemical Society*, **9**, 101–109.

438 Thy L.T.M., Cuong P.M., Tu T.H., Nam H.M., Hieu N.H. and Phong M.T. (2020), Fabrication of

439   magnetic iron oxide/graphene oxide nanocomposite for removal of lead ions from water,

440   *Chemical Engineering Transactions*, **78**, 277–282.

441 Vandevivere P.C., Bianchi R. and Verstraete W. (1998), Treatment and reuse of wastewater from

442   textile wet-processing industry: review of emerging technologies, *Journal of Chemical*

443   *Technology and Biotechnology*, **72**, 289–302.

444 Van Tran T., Nguyen D.T.C., Le H.T.N., Nguyen O.T.K., Nguyen V.H., Nguyen T.T., Bach L.G. and

445   Nguyen T.D. (2019), A hollow mesoporous carbon from metal-organic framework for robust

446   adsorbability of ibuprofen drug in water, *Royal Society Open Science*, **6**, 190058.

447 Vasiljevic Z.Z., Dojcinovic M.P., Vujancevic J.D., Jankovic-Castvan I., Ognjanovic M., Tadic N.B.,

448   Stojadinovic S., Brankovic G.O. and Nikolic M.V. (2020), Photocatalytic degradation methylene

449   blue, under natural sunlight using iron titanate nanoparticles prepared by a modified sol-gel

450   method, *Royal Society Open Science*, **7**, 1–15.

451 Wan X., Yuan M., Tie S. and Lan S. (2013), Effect of catalyst characters on photocatalytic activity

452   and process of NiO nanoparticles in the degradation of methylene blue, *Applied Surface Science*,

453   **277**, 40-46.

454 Wu Y., Shu R., Shan X., Zhang J., Shi J., Liu Y. and Zheng M. (2020), Facile design of cubic- like

455   cerium oxide nanoparticles decorated reduced graphene oxide with enhanced microwave

456   absorption properties, *Journal of Alloys and Compounds*, **817**, 152766.

457 Zhao P., Mo Z., Zhang P., Zhu X. and Guo R. (2015), Synthesis of graphene/Fe$_3$O$_4$/NiO magnetic

458   nanocomposites and its application in photocatalytic degradation the organic pollutants in

459   wastewater, *Journal of Porous Materials*, **22**, 1245–1253.

460   Ziaadini F., Mostafavia A., Shamspura T. and Fathirad F. (2019), Photocatalytic degradation of

461   Methylene blue from aqueous solution using $Fe_3O_4@SiO_2@CeO_2$ core-shell magnetic

462   nanostructure as an effective catalyst, *Advances in Environmental Technology*, **2**, 127–132.

463   Zielińska-Jurek A., Bielan Z., Dudziak S., Wolak I., Sobczak Z., Klimczuk T., Nowaczyk G. and

464   Hupka J. (2017), Design and application of magnetic photocatalysts for water treatment. The

465   effect of particle charge on surface functionality, *Catalysts*, **7**, 360.

466   Zinatloo-Ajabshir S. and Salavati-Niasari M. (2019), Preparation of magnetically retrievable

467          $CoFe_2O_4@SiO_2@Dy_2Ce_2O_7$ nanocomposites as novel photocatalyst for highly efficient

468   degradation of organic contaminants. *Composites Part B: Engineering*, **174**, 106930.

469

470